JOURNAL OF ENVIRONMENTAL SCIENCES 102 (2021) 198–206

Available online at www.sciencedirect.com

ScienceDirect

www.elsevier.com/locate/jes

JES JOURNAL OF ENVIRONMENTAL SCIENCES

www.jesc.ac.cn

Significant influences of TiO_2 crystal structures on NO_2 and HONO emissions from the nitrates photolysis

*Wenwen Xu***, *Wangjin Yang***, *Chong Han**, *He Yang*, *Xiangxin Xue*

School of Metallurgy, Northeastern University, Shenyang 110819, China

ARTICLE INFO

Article history:
Received 4 July 2020
Revised 3 September 2020
Accepted 6 September 2020
Available online 3 October 2020

Keywords:
TiO_2
Nitrates
Photolysis
NO_2

ABSTRACT

The emissions of NO_2 and HONO from the KNO_3 photolysis in the presence of TiO_2 were measured using a round-shape reactor coupled to a NO_x analyzer. TiO_2 played important roles in the emission flux density of NO_2 (R_{NO_2}) and HONO (R_{HONO}), depending on crystal structures and mass ratios of TiO_2. R_{NO_2} and R_{HONO} significantly decreased with increasing the rutile and anatase mass ratios from 0 to 8 and 0.5 wt.%, respectively. Nevertheless, with further increasing the anatase mass ratio to 8 wt.%, there was an increase in R_{NO_2} and R_{HONO}. R_{NO_2} on $KNO_3/TiO_2/SiO_2$ had positive correlation with the KNO_3 mass (1–20 wt.%), irradiation intensity (80–400 W/m^2) and temperature (278–308 K), while it had the maximum value at the relative humidity (RH) of 55%. R_{HONO} on $KNO_3/TiO_2/SiO_2$ slightly varied with the KNO_3 mass and temperature, whereas it increased with the irradiation intensity and RH. In addition, the mechanism for NO_2 and HONO emissions from the nitrates photolysis and atmospheric implications were discussed.

Introduction

Nitrates are one of the main components in atmospheric aerosols, and they account for 3%–30% and 1%–24% of fine particulate matter ($PM_{2.5}$, aerodynamic particle size <2.5 μm) mass in urban and rural regions (Revuelta et al., 2012; Wen et al., 2015), respectively. Nitrates have significant environmental and health effects. For example, nitrates can act as ice nuclei (IN) and cloud condensation nuclei (CCN) (Ishizaka and Adhikari, 2003), influencing the cloud formation and the precipitation distribution. Nitrates directly influence the earth's radiation balance by absorbing and scattering solar radiation (Laskin et al., 2019). It has been shown that respiratory diseases, circulatory diseases and malignant tumours correlate with nitrates in the atmospheric aerosols, which causes serious harm to human health (Tang et al., 2017). In addition, nitrates and HNO_3 are considered to be sinks for atmospheric nitrogen oxides (NO_x, i.e., NO and NO_2) (Ostaszewski et al., 2018; Zhou et al., 2003). Nitrates can be recycled back to the atmosphere in the forms of NO_x and nitrous acid (HONO) by the renoxification process (Baergen and Donaldson, 2013, 2016; Chen et al., 2011; Handley et al., 2007; Saliba et al., 2001; Ye et al., 2016; Zhou et al., 2003; Zhu et al., 2010).

Several studies have investigated the renoxification process of nitrates/HNO_3 (Blaszczak-Boxe and Saiz-Lopez, 2018; Kleffmann et al., 2004; McFall et al., 2018; Morenz et al., 2016; Rivera-Figueroa et al., 2003; Ye et al., 2016a; Zhou et al., 2003, 2011). For instance, the heterogeneous reaction of NO with HNO_3 generated HONO and NO_2 on silica (Rivera-

* Corresponding author.
E-mail: hanch@smm.neu.edu.cn (C. Han).
** These authors contributed equally to this work.

https://doi.org/10.1016/j.jes.2020.09.016
1001-0742/

Figueroa et al., 2003) and glass surfaces (Kleffmann et al., 2004). In particular, NO_x and HONO could be produced by the photolysis of nitrates/HNO_3 adsorbed on various surfaces, including ice (Blaszczak-Boxe and Saiz-Lopez, 2018; McFall et al., 2018), snow (Blaszczak-Boxe and Saiz-Lopez, 2018; Morenz et al., 2016), plant leaves (Zhou et al., 2003, 2011), metal sheets and construction materials (Ye et al., 2016a). The HONO photolysis is an important source of hydroxyl radicals in the atmosphere and indoor air environments (Gomez Alvarez et al., 2013; Liu et al., 2019b; Zhou et al., 2018). Hydroxyl radicals can participate in the atmospheric oxidation cycles and react with most pollutants. It was reported that 30%−60% of hydroxyl radicals in the atmosphere originate from the photolysis of HONO (Ren et al., 2003; Su et al., 2008).

At present, the contribution of nitrates photolysis to HONO still remained uncertain. A very low HONO formation was observed during the photolysis of HNO_3 adsorbed on clean quartz glass surfaces (Laufs and Kleffmann, 2016), whereas the photolysis of nitrates or nitric acids was also found to be an important daytime source of HONO in the lower atmosphere (Kleffmann, 2007; Ye et al., 2016a, 2017; Zhou et al., 2011). This uncertainty may be ascribed to the mixed states of nitrates, which generally involved with various organic and inorganic substances in the atmosphere. It has been confirmed that humic acids (Yang et al., 2018) and aluminum oxides (Rubasinghege and Grassian, 2009) enhanced the photolysis of nitrates to generate HONO and NO_x.

TiO_2 is one of important mineral oxides, and its content in atmospheric aerosols varied in the range of 0.1%−10% (Hanisch and Crowley, 2003; Ndour et al., 2009a). As an effective photocatalyst (El Zein and Bedjanian, 2012b; Ndour et al., 2008, 2009a, 2009b), TiO_2 plays significant roles in atmospheric chemistry. The conversion of NO_2 to HONO (Bedjanian and El Zein, 2012; Gandolfo et al., 2015, 2017; Gustafsson et al., 2006) and the decomposition of O_3 (Nicolas et al., 2009) on TiO_2 could be greatly enhanced under irradiation. Few studies have investigated the influences of TiO_2 on the nitrates photolysis (Ndour et al., 2009a). It was observed that TiO_2 promoted photochemical conversion of nitrates to NO and NO_2 (Ndour et al., 2009a), indicating that photoactive oxides in mineral dust were efficient for the nitrates photochemistry (Gankanda and Grassian, 2014). It should be pointed out that TiO_2 has three polymorphs including rutile, anatase and brookite (Etacheri et al., 2015; Katal et al., 2020), whereas their effects on the nitrates photolysis remain unexplored. In addition, the nitrates photolysis were carried out under ultraviolet light in previous studies (Ndour et al., 2009a). To better obtain practical data, the nitrates photolysis should be further measured under real or simulated sunlight with a continuous wavelength range.

With a round-shape reactor coupled to a NO_x analyzer, the roles of TiO_2 crystal structures in the photolysis of KNO_3 to generate NO_2 and HONO were investigated under simulated sunlight. The emission flux density of NO_2 and HONO on $KNO_3/TiO_2/SiO_2$ were measured under various environmental conditions, such as KNO_3 mass, irradiation intensity, relative humidity (RH) and temperature. A series of possible reaction pathways were proposed to explain the NO_x and HONO generation from photochemical process of $KNO_3/TiO_2/SiO_2$. Finally, the nitrates photolysis in the presence of TiO_2 for atmospheric implications were discussed.

1. Materials and methods

1.1. Materials

KNO_3 (Sinopharm Chemical Reagent Co., Ltd), TiO_2 (Macklin Biochemical Co., Ltd) and SiO_2 (Sinopharm Chemical Reagent Co., Ltd) with a total mass of 2.0 g were used to prepare the sample coating. KNO_3 (1–20 wt.%, mass ratio), TiO_2 (0–8 wt.%, mass ratio) and SiO_2 were mixed in 8.0 mL of absolute ethanol solution. SiO_2 mass was determined after setting the desired mass ratio of KNO_3 and TiO_2. A stainless steel sample dish (7.0 cm diameter) was coated with the mixture above. Then, the uniform coating was prepared by drying the mixture overnight in an oven at 373 K. NO_2 standard gas (50 ppmV in N_2, Dalian Special gasses Co., LTD) and high purity N_2 and O_2 (99.99 vol.%, Shenyang gasses Co., LTD) were used.

1.2. Round-shape reactor

A round-shape reactor with the volume of 50.2 cm^3 (1.0 cm height, 8.0 cm diameter) was used to investigate the photolysis of KNO_3, and it was fully made of stainless steel material except for the quartz window, as shown in Appendix A **Fig. S1**. A xenon lamp (500 W) with a continuous light emission in the range of 300–700 nm was used to simulate sunlight. As shown in the Appendix A **Fig. S2**, the spectrum irradiance of the xenon lamp was measured by a calibrated spectroradiometer (ULS2048CL-EVO, Avantes, Netherlands), and it was similar to the spectrum irradiance of the solar (Halle and Richard, 2006; Murphy et al., 2006; Ye et al., 2016b). It should be noted that there were very few wavelengths below 300 nm for the xenon lamp, which was almost non-existent for the solar and may have effects on the nitrates photolysis. The irradiation intensity (80–400 W/m^2) on the sample surface can be controlled by adjusting the distance between the xenon lamp and the round-shape reactor. The irradiation intensity was measured using a radiometer (FZ400, Beijing Changtuo Science and Technology Co., China). The high purity N_2 and O_2 with a total flow rate of 800 mL/min were introduced into the round-shape reactor. The relative humidity (RH, 7%−70%) was adjusted by altering the ratio of dry N_2 to wet N_2, and it was measured by a hygrometer (Center 314, Shanghai Shuangxu Electronics Co., LTD, China). The experimental temperature varied within the range of 278–308 K by circulating the temperature-controlled water at the bottom of the reactor and using the water bath outside of the reactor.

1.3. Gasses measurements

The NO_2 and NO were directly measured using a NO_x chemiluminescence analyzer (THERMO 42i, Thermo Fisher Scientific, USA), which was equipped with a molybdenum converter. Because HONO will be detected as NO_2 by the NO_x analyzer, a quartz tube (10 cm length, 0.6 cm inner diameter) filled with 1.0 g of crystalline Na_2CO_3 was connected between the round-shape reactor and the NO_x analyzer. This Na_2CO_3 tube can

capture 99% of HONO at the steady state (Han et al., 2016). NO_2, NO and HONO were detected by a bypass tube in one experiment, while NO and NO_2 were measured by the Na_2CO_3 tube in another experiment. Thus, the HONO concentration can be obtained from the difference of the NO_2 signals in two separate experiments with the same NO_x chemiluminescence analyzer. This method has been widely employed to measure the HONO concentration in previous studies (Bao et al., 2018; Brigante et al., 2008; Cazoir et al., 2014; Monge et al., 2010b; Yang et al., 2018; Zhou et al., 2018). A new Na_2CO_3 tube was installed to avoid saturation effects before each experiment. About 5% of NO_2 in the experiments was captured by the Na_2CO_3 tube, which was considered in the calculations of NO_2 and HONO emission flux density. HNO_3 could also be converted to NO_2 on the molybdenum surface and detected by the NO_x chemiluminescence analyzer (Steinbacher et al., 2007). In order to exclude HNO_3 being captured by the Na_2CO_3 tube, a quartz tube filled with NaCl was also introduced to capture gaseous HNO_3 (Yang et al., 2018). There were no differences for experimental results with or without the NaCl tube, suggesting that the formation of gaseous HNO_3 was negligible.

1.4. NO_2 and HONO emission flux density

The emission flux density (molecules/(cm^2·sec)) of NO_2 (R_{NO_2}) or HONO (R_{HONO}) was defined as the number of NO_2 or HONO molecules generated by the nitrates photolysis per unit area and time. Eqs. (1) and (2) were used to quantify the production of NO_2 and HONO during the photolysis of nitrates, respectively,

$$R_{NO_2} = \frac{V_0 \times \int_{t_1}^{t_2} (C_t^{NO_2} - C_0^{NO_2})\, dt \times N_A}{V_m \times S \times (t_2 - t_1)} \quad (1)$$

$$R_{HONO} = \frac{V_0 \times \int_{t_1}^{t_2} (C_t^{HONO} - C_0^{HONO})\, dt \times N_A}{V_m \times S \times (t_2 - t_1)} \quad (2)$$

where $C_t^{NO_2}$ and $C_0^{NO_2}$ (ppbV) are the NO_2 concentration under irradiation and the steady-state NO_2 concentration in the dark, respectively; C_t^{HONO} and C_0^{HONO} (ppbV) are the HONO concentration under irradiation and the steady-state HONO concentration in the dark, respectively; t_1 and t_2 (min) are the time when the light exposure experiment starts and ends, respectively; S (cm^2) is the geometric area of the stainless steel sample dish; V_0 (mL/min) is the volume flow of gas; V_m (L/mol) is the molar volume of gas, depending on the temperature; N_A (6.022×10^{23} mol^{-1}) is the Avogadro constant. Similar equations were also employed to obtain emission flux densities of NO_2 and HONO in the photochemical processes (Yang et al., 2020; Ye et al., 2016a). Although there were slight differences in dimensional units for emission flux densities, they were essentially the same.

1.5. Analytical methods

The light absorption abilities of TiO_2 with different crystal structures were recorded via the UV–visible diffuse reflectance spectrophotometer (UV–VIS DRS, UV-2550, Shimadzu, Japan) with $BaSO_4$ as the standard reference. Mineral components of $KNO_3/TiO_2/SiO_2$ were analyzed using the X-ray diffractometer (XRD, D/max-2500/PC, Rigaku, Japan) with Cu $K\alpha$ radiation at 40 kV and 300 mA. Appendix A **Fig. S3** displays the X-ray diffraction patterns, confirming that the sample was mainly composed of KNO_3, TiO_2 and SiO_2.

2. Results and discussion

2.1. Influences of TiO_2 crystal structures on NO_2 and HONO emissions

Appendix A **Fig. S4** shows the temporal changes of NO_2, HONO and NO signals on $KNO_3/TiO_2/SiO_2$, when rutile and anatase were used as TiO_2, respectively. Upon exposure to light, the NO_2 signal for rutile was only 0.6 ppbV (Appendix A **Fig. S4a**). By contrast, the NO_2 signal for anatase had an obvious increase at the initial stage, and then it remained unchanged at about 41 ppbV in the irradiation time of 30–60 min. This suggests that rutile and anatase play different roles in the NO_2 emission during the KNO_3 photolysis. As shown in Appendix A **Fig. S4b**, there were slight HONO emissions on $KNO_3/TiO_2/SiO_2$ under irradiation. The average HONO signal within 60 min was 0.8 and 1.0 ppbV for rutile and anatase, respectively. The NO signal was always negligible in the dark and under irradiation (Appendix A **Fig. S4c**).

Fig. 1 shows the R_{NO_2} and R_{HONO} on $KNO_3/TiO_2/SiO_2$ as a function of the rutile or anatase mass ratio. The error bars in all figures represent the standard deviations of three independent experiments. As shown in Fig. 1**a**, R_{NO_2} and R_{HONO} markedly decreased from $(2.99 \pm 0.24) \times 10^{11}$ and $(1.13 \pm 0.28) \times 10^{11}$ to $(5.72 \pm 0.34) \times 10^{9}$ and $(1.13 \pm 0.11) \times 10^{10}$ molecules/(cm^2·sec) with increasing the rutile mass ratio from 0 to 8 wt.%, respectively. It is concluded that rutile significantly inhibits the NO_2 and HONO emissions from the KNO_3 photolysis.

Compared to the rutile, the anatase presented different influences on the NO_2 and HONO emissions from the KNO_3 photolysis. Fig. 1**b** shows that R_{NO_2} and R_{HONO} decreased to 0 and $(1.46 \pm 0.03) \times 10^{10}$ molecules/(cm^2·sec), respectively, when the anatase mass ratio increased to 0.5 wt.%. Nevertheless, with further increasing the anatase mass ratio to 8 wt.%, R_{NO_2} sharply increased to $(3.31 \pm 0.13) \times 10^{11}$ molecules/(cm^2·sec), accompanied by a slight R_{HONO} increase. These results indicate that the role of anatase in the NO_2 and HONO emissions from the KNO_3 photolysis greatly depends on the anatase mass ratio.

The dependence of NO_2 and HONO emissions on the mixed crystals of TiO_2 has been investigated as shown in Appendix A **Fig. S5**, where TiO_2 consisted of rutile and anatase and its mass content was 5 wt.% in $KNO_3/TiO_2/SiO_2$. With decreasing the mass ratio of rutile to anatase from 4.0 to 0.25, R_{NO_2} continuously increased from $(0.79 \pm 0.43) \times 10^{10}$ to $(1.18 \pm 0.17) \times 10^{11}$ molecules/(cm^2·sec). By contrast, R_{HONO} almost remain unchanged within experimental uncertainties and its average value was $(1.23 \pm 0.58) \times 10^{10}$ molecules/(cm^2·sec). It means that the mixed-states of rutile and anatase have important effects on the nitrates photolysis.

The photolysis pathways of nitrates were proposed according to experimental results and previous studies

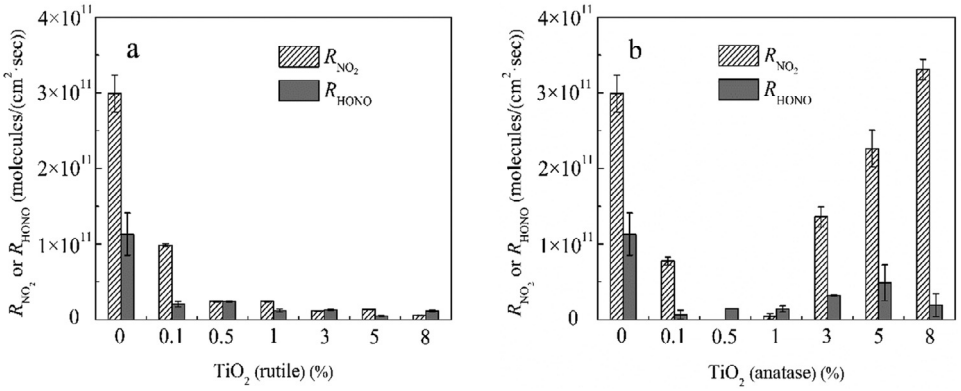

Fig. 1 – Emission flux density of NO_2 (R_{NO_2}) and HONO (R_{HONO}) on $KNO_3/TiO_2/SiO_2$ at different mass ratios of (a) rutile and (b) anatase. Reaction conditions: 10 wt.% KNO_3, irradiation intensity of 290 W/m^2, temperature of 298 K, and relative humidity (RH) of 40%.

Baergen and Donaldson, 2013; Ndour et al., 2009a; Richards-Henderson et al., 2015; Schwartz-Narbonne et al., 2019). Nitrates can accept photons and generate NO_2 and NO_2^- (Reactions (3) and (4)). HONO was produced by the protonation process of NO_2^- (Reaction (5)).

$$NO_3^- + h\upsilon \rightarrow NO_2 + O^- \quad (3)$$

$$NO_3^- + h\upsilon \rightarrow NO_2^- + O\bullet \quad (4)$$

$$NO_2^- + H^+ \rightarrow HONO \quad (5)$$

The photolysis of nitrates in the presence of TiO_2 can be explained by Reactions (6)-(9). TiO_2 accepted photons to form electron (e_{cb}^-) and hole (h_{vb}^+) pairs under irradiation (Reaction (6)) Bedjanian and El Zein, 2012; Moon et al., 2019; Ndour et al., 2009a), which would change chemical reaction channels of the nitrates photolysis (Ndour et al., 2009a). The holes (h_{vb}^+) interacted with H_2O to produce HO• and H^+ (Reaction (7)) El Zein and Bedjanian, 2012a). NO_3^- reacted with the holes (h_{vb}^+) to generate NO_3 radicals (NO_3•) (Reaction (8)) Ndour et al., 2009a), which would be decomposed to yield NO_2 and oxygen radicals (O•) under irradiation (Reaction (9)). NO_2 accepted the electrons (e_{cb}^-) to form NO_2^- (Reaction (10)) Bedjanian and El Zein, 2012), and then NO_2 and HONO would be produced by the reactions of NO_2^- with HO• (Reaction (11)) and H^+ (Reaction (5)) (Bedjanian and El Zein, 2012), respectively.

$$TiO_2 + h\upsilon \rightarrow e_{cb}^- + h_{vb}^+ + TiO_2 \quad (6)$$

$$H_2O + h_{vb}^+ \rightarrow HO\bullet + H^+ \quad (7)$$

$$NO_3^- + h_{vb}^+ \rightarrow NO_3\bullet \quad (8)$$

$$NO_3\bullet + h\upsilon \rightarrow NO_2 + O\bullet \quad (9)$$

$$NO_2 + e_{cb}^- \rightarrow NO_2^- \quad (10)$$

$$NO_2^- + HO\bullet \rightarrow NO_2 + OH^- \quad (11)$$

According to the reaction mechanism above, R_{NO_2} and R_{HONO} by the nitrates photolysis should be enhanced in the presence of TiO_2. However, compared with that on KNO_3/SiO_2, R_{NO_2} and R_{HONO} on $KNO_3/TiO_2/SiO_2$ exhibited a significant decrease, when the rutile and anatase mass ratio was less than 8 and 0.5 wt.%, respectively Fig. 1). This may be ascribed to secondary heterogeneous uptake of NO_2 and HONO generated in situ from the nitrates photolysis on the TiO_2 surface. To identify this assumption, the photochemical uptake of NO_2 on rutile and anatase was examined as shown in Appendix A **Fig. S6**. It was clearly observed that the NO_2 concentration drastically decreased upon exposure to TiO_2 under irradiation, confirming that light obviously enhanced the uptake of NO_2 on TiO_2. Previous studies also demonstrated photo-enhanced reaction of NO_2 on TiO_2 and grime (El Zein and Bedjanian, 2012a; Liu et al., 2019a, 2020; Ndour et al., 2008, 2009b). The photochemical conversions of NO_2 to HONO and HNO_3 on TiO_2 can be described using the Reactions ((6), (7), (12) and (13) (Bedjanian and El Zein, 2012; Devahasdin et al., 2003; Ndour et al., 2008; Ohko et al., 2008).

$$NO_2 + e_{cb}^- + H^+ \rightarrow HONO \quad (12)$$

$$NO_2 + HO\bullet \rightarrow HNO_3 \quad (13)$$

The KNO_3 photolysis (Fig. 1) and the secondary photochemical uptake of NO_2 on TiO_2 (Appendix A **Fig. S6**) contributed to the HONO formation. The conversion of NO_2 to HONO on the illuminated TiO_2 surface has been reported (Bedjanian and El Zein, 2012; Gustafsson et al., 2006; Monge et al., 2010a). However, the secondary uptake of HONO generated in situ can occur on the TiO_2 surface under irradiation (El Zein et al., 2013; El Zein and Bedjanian, 2012b), which led to the decrease in R_{HONO} during the KNO_3 photolysis in the presence of TiO_2. As shown in Fig. 1**b**, R_{NO_2} and R_{HONO} had an increase with the anatase mass ratio ranging from 1 to 8 wt.%, which was in contrast to the effect of rutile on R_{NO_2} and R_{HONO}. This means that anatase plays a more significant enhancement role in the KNO_3 photolysis than the secondary photochemical uptake of NO_2 and HONO at a larger anatase mass ratio. Nitrates mixed with TiO_2 are a complex reaction system,

where photolysis and photochemical uptake occur simultaneously. Both the formation of gaseous NO_2 and HONO by the nitrates photolysis (Fig. 1) and the photochemical uptake of NO_2 on rutile or anatase (Appendix A **Fig. S6**) demonstrated that NO_2 and HONO were not completely recycled back to nitrates through the photocatalytic reaction on TiO_2. Therefore, nitrates were consumed during the photolysis process in the presence of TiO_2.

To understand the reasons for different effects of rutile and anatase on the nitrates photolysis, the light absorption property of TiO_2 was measured as shown in Appendix A **Fig. S7**. According to the UV–VIS DRS, the band gap of TiO_2 was calculated and summarized in Appendix A **Table S1**. The rutile, anatase and their mixtures had similar band gap between 3.21 and 3.36 eV. The band gap of semiconductor photocatalysts determined their ability of light absorption (Ahmadi et al., 2019; Maisano et al., 2016) and the generation of electron and hole pairs (Tayade et al., 2007). This indicates that the slight difference in the light absorption property of rutile and anatase have a minor effect on their photocatalytic activity for the nitrates photolysis. The discrepancy of rutile and anatase in the influences on the nitrates photolysis may originate from their special physicochemical properties, such as surface and electronic structure (Etacheri et al., 2015; Tayade et al., 2007), stability (Etacheri et al., 2015), reduction and oxidation ability (Diebold, 2003; Henderson, 2011), and recombination rate of photo-generated electron-hole pairs (Karthikeyan et al., 2017; Katal et al., 2020). It has been proved that anatase generally had higher photocatalytic activity than rutile (Tayade et al., 2007).

2.2. *Influences of environmental factors on NO_2 and HONO emissions*

In order to further characterize the nitrates photolysis, the NO_2 and HONO emissions on KNO_3/SiO_2 mixed with rutile and anatase were measured under different environmental conditions. Fig. 2 shows R_{NO_2} and R_{HONO} as a function of the KNO_3 mass ratio. With increasing the KNO_3 mass ratio from 1 to 20 wt.%, R_{NO_2} increased from $(8.54 \pm 1.00) \times 10^{10}$ to $(1.82 \pm 0.21) \times 10^{11}$ molecules/(cm^2·sec). R_{HONO} had a slight increase with the KNO_3 mass ratio ranging from 1 to 5 wt.%, while it almost remained unchanged at $(1.96 \pm 0.34) \times 10^{10}$ molecules/(cm^2·sec) in the KNO_3 mass range of 5–20 wt.%.

Fig. 3 displays R_{NO_2} and R_{HONO} on $KNO_3/TiO_2/SiO_2$ at different irradiation intensity. R_{NO_2} and R_{HONO} exhibited an increase trend with irradiation intensity. R_{NO_2} and R_{HONO} increased from $(5.32 \pm 0.30) \times 10^{10}$ and $(1.06 \pm 0.56) \times 10^{10}$ molecules/(cm^2·sec) at 80 W/m^2 to $(1.49 \pm 0.28) \times 10^{11}$ and $(4.61 \pm 0.81) \times 10^{10}$ molecules/(cm^2·sec) at 400 W/m^2, respectively. The increase of irradiation intensity provided more photons for the KNO_3 photolysis and the generation of electron and hole pairs on TiO_2, which led to more NO_2 and HONO emissions by Reactions (3)–(11).

As shown in Fig. 4, both R_{NO_2} and R_{HONO} increased with RH ranging from 7% to 55%, and decreased from 55% to 70% RH. The maximum values of R_{NO_2} and R_{HONO} at RH = 55% were $(1.69 \pm 0.08) \times 10^{11}$ and $(2.98 \pm 1.65) \times 10^{10}$ molecules/(cm^2·sec), respectively. The increase in RH would enhance the formation of •OH and H^+ by the reaction of H_2O with h^+_{vb} (Reaction (7)) (Ndour et al., 2009a). Thus, more NO_2 and HONO was produced by the reaction of NO_2^- with •OH (Reaction 11)) and the protonation process of NO_2^- with H^+ (Reaction (5)), respectively. This contributes to the increase in R_{NO_2} and R_{HONO} with RH in the range of 7%–55%. It has been reported that the photolysis of nitrates under humid conditions was faster than that under dry conditions (Rubasinghege and Grassian, 2009). The scavenging of the holes (h^+_{vb}) by H_2O (Reaction (7)) was enhanced when the RH continuously increased to 70% (Ndour et al., 2009a). This would inhibit the reaction of NO_3^- and h^+_{vb} to produce NO_3• (Reaction (8)), hindering the formation of NO_2 and HONO in Reactions (9–11). In addition, the disproportionation reaction between NO_2 and H_2O adsorbed on the surface became more significant. More NO_2^- and HONO would be dissolved in the adsorbed H_2O. Accordingly, R_{NO_2} and R_{HONO} decreased with increasing the RH to 70%.

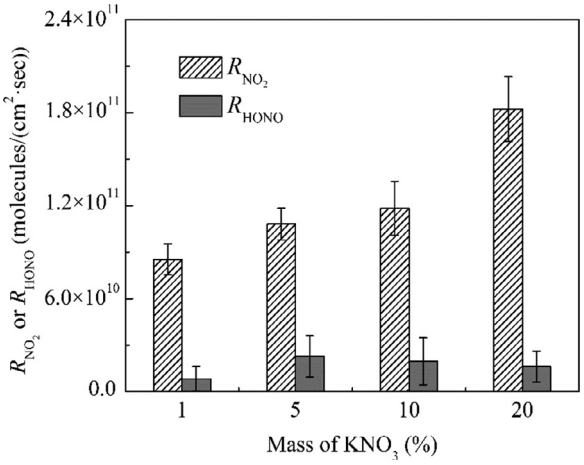

Fig. 2 – R_{NO_2} and R_{HONO} on $KNO_3/TiO_2/SiO_2$ at different KNO_3 mass ratios. Reaction conditions: 5 wt.% TiO_2 (the mass ratio of rutile to anatase was 1:4), irradiation intensity of 290 W/m^2, temperature of 298 K, and RH of 40%.

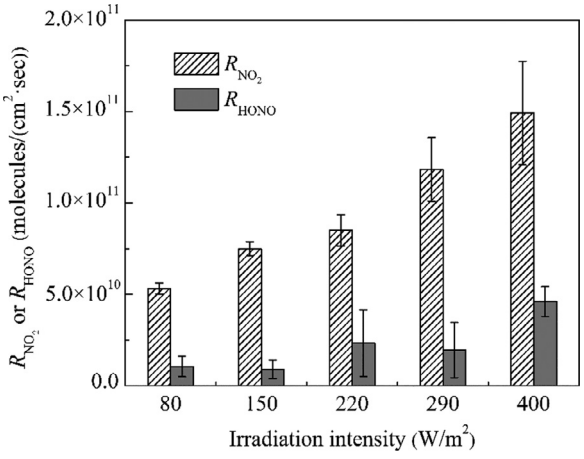

Fig. 3 – R_{NO_2} and R_{HONO} on $KNO_3/TiO_2/SiO_2$ at different irradiation intensity. Reaction conditions: 10 wt.% KNO_3, 5 wt.% TiO_2 (the mass ratio of rutile to anatase was 1:4), temperature of 298 K, and RH of 40%.

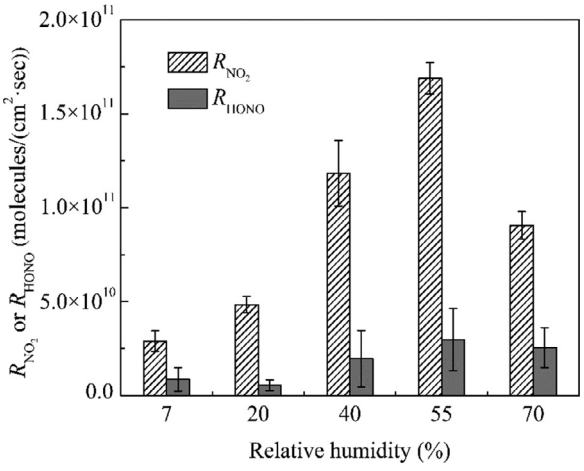

Fig. 4 – R_{NO_2} and R_{HONO} on $KNO_3/TiO_2/SiO_2$ at different relative humidity. Reaction conditions: 10 wt.% KNO_3, 5 wt.% TiO_2 (the mass ratio of rutile to anatase was 1:4), irradiation intensity of 290 W/m^2, and temperature of 298 K.

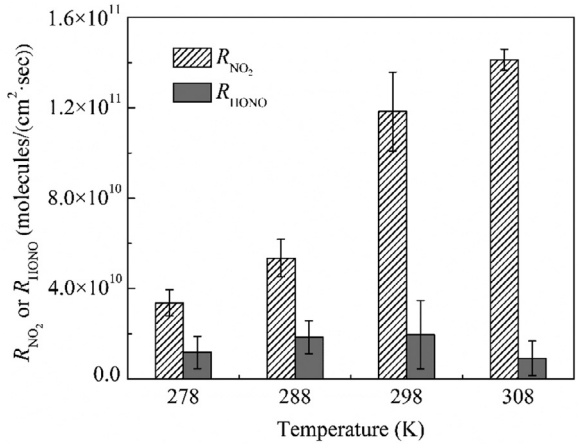

Fig. 5 – R_{NO_2} and R_{HONO} on $KNO_3/TiO_2/SiO_2$ at different temperature. Reaction conditions: 10 wt.% KNO_3, 5 wt.% TiO_2 (the mass ratio of rutile to anatase was 1:4), irradiation intensity of 290 W/m^2, and RH of 40%.

Fig. 5 summarizes the changes of R_{NO_2} and R_{HONO} as a function of temperature. R_{NO_2} increased from (3.36 ± 0.58) × 10^{10} molecules/(cm^2·sec) at 278 K to (1.41 ± 0.05) × 10^{11} molecules/(cm^2·sec) at 308 K. R_{HONO} had a slight variation at 278–308 K, with an average value of (1.47 ± 0.51) × 10^{10} molecules/(cm^2·sec). This means that some reaction pathways to generate NO_2 may be thermally controlled, such as the reaction of NO_2^- with •OH (Reaction (11)). Field study also found that strong thermal decomposition in summer resulted in a significant reduction of nitrates levels (Revuelta et al., 2012), which seemed to be consistent with the findings reported here.

3. Conclusions and atmospheric implications

The rutile and anatase had different effects on R_{NO_2} and R_{HONO}, suggesting significant dependence of the KNO_3 photolysis on TiO_2 crystal structures. The NO_2 and HONO emissions from the KNO_3 photolysis relied on various environmental conditions, including KNO_3 mass, irradiation intensity, temperature and RH. These findings would be helpful to understand the atmospheric lifetime of nitrates and the role of nitrates in the reservoirs of NO_2 and HONO in the real environment.

The atmospheric lifetime (τ) of nitrates can be calculated by the following equations (Ye et al., 2017),

$$N_{\text{nitrates}} = N_{\text{nitrates, total}} \times \frac{h}{H} \tag{14}$$

$$H = \frac{m}{\rho \times S} \tag{15}$$

$$J_{\text{nitrates}} = \frac{(R_{NO_2} \times M_{NO_2} + R_{HONO} \times M_{HONO}) \times S}{N_A \times N_{\text{nitrates}}} \tag{16}$$

$$\tau = \frac{1}{J_{\text{nitrates}}} \tag{17}$$

where N_{nitrates} (g) is the mass of nitrates photolyzed in the reaction; $N_{\text{nitrates, total}}$ (g) is the total mass of nitrates used in the experiments; h (nm) is the nitrates coating thickness where light can reach, and it was assumed to be 100 nm; H is the total thickness of the sample coating containing TiO_2 (231.40 μm) or without TiO_2 (237.40 μm); m (g) is the total mass of sample; ρ is the mixture density of $KNO_3/TiO_2/SiO_2$ (2.247 g/cm^3) or KNO_3/SiO_2 (2.19 g/cm^3), which is calculated according to the density and the mass ratio of each substance; S (cm^2) is the geometric area of the stainless steel sample dish; J_{nitrates} (sec^{-1}) is the photolysis rate constant; M_{NO_2} (g/mol) and M_{HONO} (g/mol) are the molar mass of NO_2 and HONO, respectively. Under environmental conditions with irradiation intensity of 290 W/m^2, 298 K, 40% RH, KNO_3 mass of 10 wt.% and TiO_2 mass of 5 wt.% (the mass ratio of rutile to anatase was 1:4), the photolysis rate constant and atmospheric lifetime of nitrates were calculated to be 3.6 × 10^{-6}–5.8 × 10^{-6} sec^{-1} and 47.9–77.2 hr, respectively. They were estimated to be 1.3 × 10^{-5}–1.6 × 10^{-5} sec^{-1} and 17.4–21.4 hr in the absence of TiO_2, respectively. This photolysis rate constant was larger than that with TiO_2, which was ascribed to lower NO_2 and HONO emissions due to their secondary photochemical uptake on TiO_2. The photolysis rate constants obtained here were within the range (6.0 × 10^{-6}–5.0 × 10^{-4} sec^{-1}) of that of nitrates and nitric acids in low-NO_x environments (Ye et al., 2016a, 2017; Zhou et al., 2003). The calculated atmospheric lifetime of nitrates without TiO_2 was close to that (15 hr) of total nitrates in real atmospheric aerosols (Ye et al., 2017).

Assuming the aerosol surface concentration of 10^2–10^3 μm^2/cm^3 (Stemmler et al., 2007) and the nitrates content of 10 wt.% in the continental aerosols (Poulain et al., 2011; Revuelta et al., 2012; van Pinxteren et al., 2009; Wang et al., 2015), the source strength of NO_2 and HONO from the photolysis of nitrates in aerosols without TiO_2 was estimated

to be 3.7–43.2 and 1.1–18.9 pptV/hr under the environmental conditions above, respectively. For the nitrates photolysis in aerosols containing TiO_2, it was calculated to be 1.4–18.1 and 0.1–4.6 pptV/hr for NO_2 and HONO, respectively. The NO_2 formation (30 pptV/hr) from the photolysis of HNO_3 deposited on the ground and vegetation surfaces was within the source strength of NO_2 from the photolysis of nitrates with or without TiO_2 (Zhou et al., 2003). The HONO source strength was 70–200 pptV/hr (Sörgel et al., 2015; Zhang et al., 2012; Zhou et al., 2011) and 1–10 ppbV/hr (Elshorbany et al., 2010; Villena et al., 2011) in rural areas and urban areas, respectively, which was much greater than the HONO formation from the photolysis of nitrates with or without TiO_2. This work clearly confirmed that TiO_2 played important roles in NO_2 and HONO emissions from the nitrates photolysis. Other minerals with photocatalytic activity, such as Fe_2O_3 and ZnO, should be also further investigated to determine their influences on the nitrates photolysis.

Acknowledgments

This research was financially supported by the LiaoNing Revitalization Talents Program (No. XLYC1907185) and the Fundamental Research Funds for the Central Universities (Nos. N182505040 and N2025011).

Appendix A. Supplementary data

Supplementary material associated with this article can be found in the online version at doi:10.1016/j.jes.2020.09.016.

REFERENCES

Ahmadi, M., Dorraji, M.S.S., Rasoulifard, M.H., Amani-Ghadim, A.R., 2019. The effective role of reduced-graphene oxide in visible light photocatalytic activity of wide band gap $SrTiO_3$ semiconductor. Sep. Purif. Technol. 228, 115771.

Baergen, A.M., Donaldson, D.J., 2013. Photochemical renoxification of nitric acid on real urban grime. Environ. Sci. Technol. 47, 815–820.

Baergen, A.M., Donaldson, D.J., 2016. Formation of reactive nitrogen oxides from urban grime photochemistry. Atmos. Chem. Phys. 16, 6355–6363.

Bao, F.X., Li, M., Zhang, Y., Chen, C.C., Zhao, J.C., 2018. Photochemical aging of Beijing urban $PM_{2.5}$: HONO production. Environ. Sci. Technol. 52, 6309–6316.

Bedjanian, Y., El Zein, A., 2012. Interaction of NO_2 with TiO_2 surface under UV irradiation: products study. J. Phys. Chem. A 116, 1758–1764.

Blaszczak-Boxe, C.S., Saiz-Lopez, A., 2018. Nitrate photolysis in ice and snow: a critical review of its multiphase chemistry. Atmos. Environ. 193, 224–241.

Brigante, M., Cazoir, D., D'Anna, B., George, C., Donaldson, D.J., 2008. Photoenhanced uptake of NO_2 by pyrene solid films. J. Phys. Chem. A 112, 9503–9508.

Cazoir, D., Brigante, M., Ammar, R., D'Anna, B., George, C., 2014. Heterogeneous photochemistry of gaseous NO_2 on solid fluoranthene films: a source of gaseous nitrous acid (HONO) in the urban environment. J. Photochem. Photobiol. A Chem. 273, 23–28.

Chen, H.H., Navea, J.G., Young, M.A., Grassian, V.H., 2011. Heterogeneous photochemistry of trace atmospheric gases with components of mineral dust aerosol. J. Phys. Chem. A 115, 490–499.

Devahasdin, S., Fan, C., Li, K.Y., Chen, D.H., 2003. TiO_2 photocatalytic oxidation of nitric oxide: transient behavior and reaction kinetics. J. Photochem. Photobiol. A Chem. 156, 161–170.

Diebold, U., 2003. The surface science of titanium dioxide. Surf. Sci. Rep. 48, 53–229.

El Zein, A., Bedjanian, Y., 2012a. Interaction of NO_2 with TiO_2 surface under UV irradiation: measurements of the uptake coefficient. Atmos. Chem. Phys. 12, 1013–1020.

El Zein, A., Bedjanian, Y., 2012b. Reactive uptake of HONO to TiO_2 surface: "dark" reaction. J. Phys. Chem. A 116, 3665–3672.

El Zein, A., Bedjanian, Y., Romanias, M.N., 2013. Kinetics and products of HONO interaction with TiO_2 surface under UV irradiation. Atmos. Environ. 67, 203–210.

Elshorbany, Y.F., Kleffmann, J., Kurtenbach, R., Lissi, E., Rubio, M., Villena, G., et al., 2010. Seasonal dependence of the oxidation capacity of the city of Santiago de Chile. Atmos. Environ. 44, 5383–5394.

Etacheri, V., Di Valentin, C., Schneider, J., Bahnemann, D., Pillai, S.C., 2015. Visible-light activation of TiO_2 photocatalysts: advances in theory and experiments. J. Photochem. Photobiol. C 25, 1–29.

Gandolfo, A., Bartolomei, V., Gomez Alvarez, E., Tlili, S., Gligorovski, S., Kleffmann, J., et al., 2015. The effectiveness of indoor photocatalytic paints on NO_x and HONO levels. Appl. Catal. B 166, 84–90.

Gandolfo, A., Rouyer, L., Wortham, H., Gligorovski, S., 2017. The influence of wall temperature on NO_2 removal and HONO levels released by indoor photocatalytic paints. Appl. Catal. B 209, 429–436.

Gankanda, A., Grassian, V.H., 2014. Nitrate photochemistry on laboratory proxies of mineral dust aerosol: wavelength dependence and action spectra. J. Phys. Chem. A 118, 29117–29125.

Gomez Alvarez, E., Amedro, D., Afif, C., Gligorovski, S., Schoemaecker, C., Fittschen, C., et al., 2013. Unexpectedly high indoor hydroxyl radical concentrations associated with nitrous acid. Proc. Natl. Acad. Sci. USA 110, 15848 15848.

Gustafsson, R.J., Orlov, A., Griffiths, P.T., Cox, R.A., Lambert, R.M., 2006. Reduction of NO_2 to nitrous acid on illuminated titanium dioxide aerosol surfaces: implications for photocatalysis and atmospheric chemistry. Chem. Commun. 3936–3938.

Halle, A.T., Richard, C. , 2006. Simulated solar light irradiation of mesotrione in natural waters. Environ. Sci. Technol. 40, 3842–3847.

Han, C., Yang, W.J., Wu, Q.Q., Yang, H., Xue, X.X., 2016. Heterogeneous photochemical conversion of NO_2 to HONO on the humic acid surface under simulated sunlight. Environ. Sci. Technol. 50, 5017–5023.

Handley, S.R., Clifford, D., Donaldson, D.J., 2007. Photochemical loss of nitric acid on organic films: a possible recycling mechanism for NO_x. Environ. Sci. Technol. 41, 3898–3903.

Hanisch, F., Crowley, J.N., 2003. Ozone decomposition on Saharan dust: an experimental investigation. Atmos. Chem. Phys. 3, 119–130.

Henderson, M.A., 2011. A surface science perspective on TiO_2 photocatalysis. Surf. Sci. Rep. 66, 185–297.

Ishizaka, Y., Adhikari, M., 2003. Composition of cloud condensation nuclei. J. Geophys. Res.: Atmos. 108, 4138.

Karthikeyan, V., Maniarasu, S., Manjunath, V., Ramasamy, E., Veerappan, G., 2017. Hydrothermally tailored anatase TiO_2 nanoplates with exposed {111} facets for highly efficient dye-sensitized solar cells. Sol. Energy 147, 202–208.

Katal, R., Masudy-Panah, S., Tanhaei, M., Farahani, M.H.D.A.,

Hu, J.Y., 2020. A review on the synthesis of the various types of anatase TiO_2 facets and their applications for photocatalysis. Chem. Eng. J. 384, 123384.
Kleffmann, J., Benter, T., Wiesen, P., 2004. Heterogeneous reaction of nitric acid with nitric oxide on glass surfaces under simulated atmospheric conditions. J. Phys. Chem. A 108, 5793–5799.
Kleffmann, J., 2007. Daytime sources of nitrous acid (HONO) in the atmospheric boundary layer. ChemPhysChem 8, 1137–1144.
Laskin, A., Moffet, R.C., Gilles, M.K., 2019. Chemical imaging of atmospheric particles. Acc. Chem. Res. 52, 3419–3431.
Laufs, S., Kleffmann, J., 2016. Investigations on HONO formation from photolysis of adsorbed HNO_3 on quartz glass surfaces. Phys. Chem. Chem. Phys. 18, 9616–9625.
Liu, J.P., Deng, H.F., Li, S., Jiang, H.Y., Mekic, M., Zhou, W.T., et al., 2020. Light-enhanced heterogeneous conversion of NO_2 to HONO on solid films consisted of fluorene and fluorene/Na_2SO_4: an impact on urban and indoor atmosphere. Environ. Sci. Technol. 54 (18), 11079–11086.
Liu, J.P., Li, S., Mekic, M., Jiang, H.Y., Zhou, W.T., Loisel, G., et al., 2019a. Photoenhanced uptake of NO_2 and HONO formation on real urban grime. Environ. Sci. Technol. Lett. 6, 413–417.
Liu, J.P., Li, S., Zeng, J.F., Mekic, M., Yu, Z.J., Zhou, W.T., et al., 2019b. Assessing indoor gas phase oxidation capacity through real-time measurements of HONO and NO_x in Guangzhou, China. Environ. Sci. Process. Impacts 21, 1393–1402.
Maisano, M., Dozzi, M.V., Selli, E., 2016. Searching for facet-dependent photoactivity of shape-controlled anatase TiO_2. J. Photochem. Photobiol. C 28, 29–43.
McFall, A.S., Edwards, K.C., Anastasio, C., 2018. Nitrate photochemistry at the air-ice interface and in other ice reservoirs. Environ. Sci. Technol. 52, 5710–5717.
Monge, M.E., D'Anna, B., George, C., 2010a. Nitrogen dioxide removal and nitrous acid formation on titanium oxide surfaces-an air quality remediation process? Phys. Chem. Chem. Phys 12, 8991–8998.
Monge, M.E., D'Anna, B., Mazri, L., Giroir-Fendler, A., Ammann, M., Donaldson, D.J., et al., 2010b. Light changes the atmospheric reactivity of soot. Proc. Natl. Acad. Sci. USA 107, 6605–6609.
Moon, D.R., Ingham, T., Whalley, L.K., Seakins, P.W., Baeza-Romero, M.T., Heard, D.E., 2019. Production of HO_2 and OH radicals from near-UV irradiated airborne TiO_2 nanoparticles. Phys. Chem. Chem. Phys. 21, 2325–2336.
Morenz, K.J., Shi, Q.W., Murphy, J.G., Donaldson, D.J., 2016. Nitrate photolysis in salty snow. J. Phys. Chem. A 120, 7902–7908.
Murphy, A.B., Barnes, P.R.F., Randeniya, L.K., Plumb, I.C., Grey, I.E., Horne, M.D., et al., 2006. Efficiency of solar water splitting using semiconductor electrodes. Int. J. Hydrog. Energy 31, 1999–2017.
Ndour, M., D'Anna, B., George, C., Ka, O., Balkanski, Y., Kleffmann, J., et al., 2008. Photoenhanced uptake of NO_2 on mineral dust: laboratory experiments and model simulations. Geophy. Res. Lett. 35, L05812.
Ndour, M., Conchon, P., D'Anna, B., Ka, O., George, C., 2009a. Photochemistry of mineral dust surface as a potential atmospheric renoxification process. Geophy. Res. Lett. 36, L05816.
Ndour, M., Nicolas, M., D'Anna, B., Ka, O., George, C., 2009b. Photoreactivity of NO_2 on mineral dusts originating from different locations of the Sahara desert. Phys. Chem. Chem. Phys. 11, 1312–1319.
Nicolas, M., Ndour, M., Ka, O., D'Anna, B., George, C., 2009. Photochemistry of atmospheric dust: ozone decomposition on illuminated titanium dioxide. Environ. Sci. Technol. 43, 7437–7442.
Ohko, Y., Nakamura, Y., Fukuda, A., Matsuzawa, S., Takeuchi, K., 2008. Photocatalytic oxidation of nitrogen dioxide with TiO_2 thin films under continuous UV-light illumination. J. Phys. Chem. A 112, 10502–10508.
Ostaszewski, C.J., Stuart, N.M., Lesko, D.M.B., Kim, D., Lueckheide, M.J., Navea, J.G., 2018. Effects of coadsorbed water on the heterogeneous photochemistry of nitrates adsorbed on TiO_2. J. Phys. Chem. A 122, 6360–6371.
Poulain, L., Spindler, G., Birmili, W., Plass-Dulmer, C., Wiedensohler, A., Herrmann, H., 2011. Seasonal and diurnal variations of particulate nitrate and organic matter at the IfT research station melpitz. Atmos. Chem. Phys. 11, 12579–12599.
Ren, X.R., Harder, H., Martinez, M., Lesher, R.L., Oliger, A., Simpas, J.B., et al., 2003. OH and HO_2 Chemistry in the urban atmosphere of New York City. Atmos. Environ. 37, 3639–3651.
Revuelta, M.A., Harrison, R.M., Nunez, L., Gomez-Moreno, F.J., Pujadas, M., Artinano, B., 2012. Comparison of temporal features of sulphate and nitrate at urban and rural sites in Spain and the UK. Atmos. Environ. 60, 383–391.
Richards-Henderson, N.K., Anderson, C., Anastasio, C., Finlayson-Pitts, B.J., 2015. The effect of cations on NO_2 production from the photolysis of aqueous thin water films of nitrate salts. Phys. Chem. Chem. Phys. 17, 32211–32218.
Rivera-Figueroa, A.M., Sumner, A.L., Finlayson-Pitts, B.J., 2003. Laboratory studies of potential mechanisms of renoxification of tropospheric nitric acid. Environ. Sci. Technol. 37, 548–554.
Rubasinghege, G., Grassian, V.H., 2009. Photochemistry of adsorbed nitrate on aluminum oxide particle surfaces. J. Phys. Chem. A 113, 7818–7825.
Saliba, N.A., Yang, H., Finlayson-Pitts, B.J., 2001. Reaction of gaseous nitric oxide with nitric acid on silica surfaces in the presence of water at room temperature. J. Phys. Chem. A 105, 10339–10346.
Schwartz-Narbonne, H., Jones, S.H., Donaldson, D.J., 2019. Indoor lighting releases gas phase nitrogen oxides from indoor painted surfaces. Environ. Sci. Technol. Lett. 6, 92–97.
Sörgel, M., Trebs, I., Wu, D., Held, A., 2015. A comparison of measured HONO uptake and release with calculated source strengths in a heterogeneous forest environment. Atmos. Chem. Phys. 15, 9237–9251.
Steinbacher, M., Zellweger, C., Schwarzenbach, B., Bugmann, S., Buchmann, B., Ordóñez, C., et al., 2007. Nitrogen oxide measurements at rural sites in Switzerland: bias of conventional measurement techniques. J. Geophys. Res.: Atmos. 112, D11307.
Stemmler, K., Ndour, M., Elshorbany, Y., Kleffmann, J., D'Anna, B., George, C., et al., 2007. Light induced conversion of nitrogen dioxide into nitrous acid on submicron humic acid aerosol. Atmos. Chem. Phys. 7, 4237–4248.
Su, H., Cheng, Y.F., Shao, M., Gao, D.F., Yu, Z.Y., Zeng, L.M., et al., 2008. Nitrous acid (HONO) and its daytime sources at a rural site during the 2004 PRIDE-PRD experiment in China. J. Geophys. Res.: Atmos. 113, D14312.
Tang, G.Q., Zhao, P.S., Wang, Y.H., Gao, W.K., Cheng, M.T., Xin, J.Y., et al., 2017. Mortality and air pollution in Beijing: the long-term relationship. Atmos. Environ. 150, 238–243.
Tayade, R.J., Surolia, P.K., Kulkarni, R.G., Jasra, R.V., 2007. Photocatalytic degradation of dyes and organic contaminants in water using nanocrystalline anatase and rutile TiO_2. Sci. Technol. Adv. Mater. 8, 455–462.
van Pinxteren, D., Brüggemann, E., Gnauk, T., Iinuma, Y., Müller, K., Nowak, A., et al., 2009. Size- and time-resolved chemical particle characterization during CAREBeijing-2006: different pollution regimes and diurnal profiles. J. Geophys. Res.: Atmos. 114, D00G09 .

Villena, G., Kleffmann, J., Kurtenbach, R., Wiesen, P., Lissi, E., Rubio, M.A., et al., 2011. Vertical gradients of HONO, NO_x and O_3 in Santiago de Chile. Atmos. Environ. 45, 3867–3873.
Wang, H.L., Zhu, B., Shen, L.J., Xu, H.H., An, J.L., Xue, G.Q., et al., 2015. Water-soluble ions in atmospheric aerosols measured in five sites in the Yangtze River Delta, China: size-fractionated, seasonal variations and sources. Atmos. Environ. 123, 370–379.
Wen, L.A., Chen, J.M., Yang, L.X., Wang, X.F., Xu, C.H., Sui, X.A., et al., 2015. Enhanced formation of fine particulate nitrate at a rural site on the North China Plain in summer: the important roles of ammonia and ozone. Atmos. Environ. 101, 294–302.
Yang, W.J., Han, C., Yang, H., Xue, X.X., 2018. Significant HONO formation by the photolysis of nitrates in the presence of humic acids. Environ. Pollut. 243, 679–686.
Yang, W.J., Yuan, H., Han, C., Yang, H., Xue, X.X., 2020. Photochemical emissions of HONO, NO_2 and NO from the soil surface under simulated sunlight. Atmos. Environ. 234, 117596.
Ye, C.X., Gao, H.L., Zhang, N., Zhou, X.L., 2016a. Photolysis of nitric acid and nitrate on natural and artificial surfaces. Environ. Sci. Technol. 50, 3530–3536.
Ye, C.X., Zhou, X.L., Pu, D., Stutz, J., Festa, J., Spolaor, M., et al., 2016b. Rapid cycling of reactive nitrogen in the marine boundary layer. Nature 532, 489–491.
Ye, C.X., Zhang, N., Gao, H.L., Zhou, X.L., 2017. Photolysis of particulate nitrate as a source of HONO and NO_x. Environ. Sci. Technol. 51, 6849–6856.
Zhang, N., Zhou, X.L., Bertman, S., Tang, D., Alaghmand, M., Shepson, P.B., et al., 2012. Measurements of ambient HONO concentrations and vertical HONO flux above a northern Michigan forest canopy. Atmos. Chem. Phys. 12, 8285–8296.
Zhou, S., Young, C.J., VandenBoer, T.C., Kowal, S.F., Kahan, T.F., 2018. Time-resolved measurements of nitric oxide, nitrogen dioxide, and nitrous acid in an occupied New York home. Environ. Sci. Technol. 52, 8355–8364.
Zhou, X.L., Gao, H.L., He, Y., Huang, G., Bertman, S.B., Civerolo, K., et al., 2003. Nitric acid photolysis on surfaces in low-NO_x environments: significant atmospheric implications. Geophys. Res. Lett. 30, 2217.
Zhou, X.L., Zhang, N., TerAvest, M., Tang, D., Hou, J., Bertman, S.B., et al., 2011. Nitric acid photolysis on forest canopy surface as a source for tropospheric nitrous acid. Nat. Geosci. 4, 440–443.
Zhu, C.Z., Xiang, B., Chu, L.T., Zhu, L., 2010. 308nm photolysis of nitric acid in the gas phase, on aluminum surfaces, and on ice films. J. Phys. Chem. A 114, 2561–2568.